

A Polariton Graph Simulator

Pavlos G. Lagoudakis^{1,2} and Natalia G. Berloff^{1,3,*}

¹Skolkovo Institute of Science and Technology Novaya St., 100, Skolkovo 143025, Russian Federation

²Department of Physics and Astronomy, University of Southampton, Southampton, SO17 1BJ, United Kingdom

³Department of Applied Mathematics and Theoretical Physics, University of Cambridge, Cambridge CB3 0WA, United Kingdom

E-mail: N.G.Berloff@damtp.cam.ac.uk

7 May 2017

Abstract. We discuss polariton graphs as a new platform for simulating the classical XY and Kuramoto models. Polariton condensates can be imprinted into any two-dimensional graph by spatial modulation of the pumping laser. Polariton simulators have the potential to reach the global minimum of the XY Hamiltonian in a bottom-up approach by gradually increasing excitation density to threshold or to study large scale synchronisation phenomena and dynamical phase transitions when operating above the threshold. We consider the modelling of polariton graphs using the complex Ginzburg-Landau model and derive analytical solutions for a single condensate, the XY model, two-mode model and the Kuramoto model establishing the relationships between them.

1. Introduction

Engineering a physical system to reproduce a many-body Hamiltonian has been at the heart of Richard P. Feynman's idea of an analogue Hamiltonian simulator [1]. Such simulators could address problems that cannot be solved by a conventional Turing classical computer, which would allow us to test various models of lattice systems or discover new states of matter. Analogue Hamiltonian simulations led to the observation of a superfluid-insulator phase transition in ultracold Bose gases that is closely related to metal-insulator transition in condensed-matter materials [2]. In the last decade various other systems have been proposed as classical or quantum simulators: ultracold bosonic and fermionic atoms and molecular gases in optical lattices [3, 4, 5, 6], photons [7], trapped ions [8, 9], superconducting q-bits [10], network of optical parametric oscillators (OPOs) [11, 12], and coupled lasers [13] among other systems.

The design of an analogue Hamiltonian simulator consists of several important ingredients [14]: (i) mapping of the Hamiltonian of the system to be simulated into the elements of the simulator and the interactions between them; (ii) preparation of the simulator in a state that is relevant to the physical problem of interest: one could be

interested in finding the ground or excited equilibrium state at a finite temperature; (iii) performing measurements on the simulator with the required precision. One of the platforms that have recently been explored is based on exciton-polariton lattices. Exciton-polaritons (or polaritons) are the composed light-matter bosonic quasi-particles formed in the strong exciton-photon coupling regime in semiconductor microcavities [15]. Under non-resonant optical excitation, free carriers relax, scatter, emit phonons and when the particle density reaches quantum degeneracy threshold, polaritons condense in the same state [16], driven by bosonic stimulation [17]. The steady state of such a condensate is characterized by the balance of pumping and dissipation of photons that decay through the Bragg reflectors carrying all information of the corresponding polariton state wavefunction such as the energy, momentum, density, phase and spin. This information allows for the in-situ characterisation of a polariton condensate in its steady state and during any dynamical transition. The non-equilibrium nature of polariton condensates gives rise to pattern formation in these systems that has been a subject of many investigations, for review see Refs. [18, 19]. Several methods for imprinting polariton lattices have been proposed. To introduce a photonic trap a partial [20] or complete etching [21] can be used. A thin-metal film technique on a grown wafer has been used to weakly modulate in-plane one-dimensional photon lattice [22]. Exciton trap states have been explored by introducing a mechanical strain in a sample [23] or by applying electric or magnetic fields that change the exciton energy [24]. Polariton condensates can be created at the vertices of any two-dimensional graph by spatial modulation of the pumping source. The first theoretical proposal [25] and its experimental realization [26, 27] to imprint polariton condensates in multi-site configurations were focused on the states, such as vortex lattices, created by the outflowing polaritons from the condensate sites. Next question concerned the way the coherence is established between the various condensates. As the excitation intensity is increased from below polaritons at the lattice site i start to condense with the wavefunction $\psi_i = \sqrt{\rho_i(\mathbf{r})} \exp[iS_i(\mathbf{r})]$, characterized by the number density $\rho_i(\mathbf{r})$ and a phase $S_i(\mathbf{r})$ with the relative phase-configuration that carries the highest polariton occupation due to the bosonic stimulation during the condensate formation [28]. By controlling the pumping intensity and profile, the graph geometry and the separation distance between the lattice sites one can control the couplings between the sites and realise various phase configurations that minimize the XY model as was shown in [29]. This gives rise to the use of the polariton graph as an analogue XY Hamiltonian simulator. The search for the global minimum of the XY Hamiltonian is via a bottom-up approach which has an advantage over classical or quantum annealing techniques, where the global ground state is reached through either a transition over metastable excited states or via tunnelling between the states in time that depends on the size of the system. Figure 1(a) shows the schematics of the classical thermal annealing, quantum annealing via tunnelling between the metastable states and the bosonic stimulation.

The XY model has been previously simulated by other physical systems: ultra cold atomic optical lattices [30] and coupled photon lasers network [13]. Polariton graphs

are as scalable as these platforms regarding the number of nodes it can involve. In Ref. [29] we have shown the graphs that consist of 45 nodes. Polariton graphs enjoy higher flexibility in engineering any geometrical configuration of nodes, since in optical lattices and laser networks it is harder going beyond a regular lattice configuration for the arrangement of the vertices. In a microcavity used in Ref.[29] there is only one longitudinal mode resonant to the exciton energy and thus the system can operate at threshold more stably than photonic laser which contains a large number of longitudinal modes within the gain bandwidth. Also, the large number of modes competing for lasing necessitates pumping much above a threshold for stable operation. This suggests that polariton graphs have an advantage over other systems for finding the ground state of XY models. Figure 1(b) shows the schematical difference between operating at the threshold and well above the threshold for finding the global minimum of the energy landscape which in our case is represented by the XY Hamiltonian.

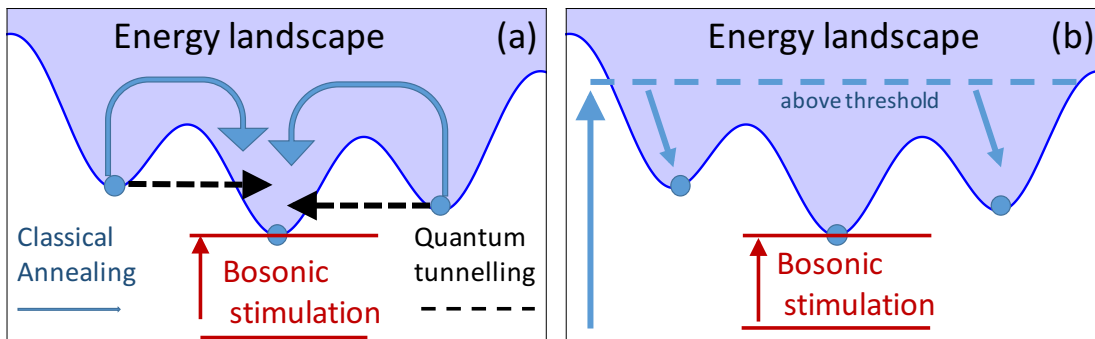


Figure 1. (a) Schematics of different types of annealing for finding the global minimum of the energy landscape of the simulated XY Hamiltonian: classical annealing via the thermal activation, quantum annealing via quantum tunnelling during the adiabatic adjustment of the simulated Hamiltonian and the bosonic stimulation that leads to the system condensation at the threshold. (b) Schematics of the comparison between photon laser and polariton graph operation.

The interest in using an analogue simulator for finding the global minimum of the XY Hamiltonian is motivated by the recent result in the theory of quantum complexity: there exist universal Hamiltonians such that all other classical spin models can be reproduced within such a model, and certain simple Hamiltonians such as the 2D Ising model with fields on a square grid with only nearest neighbour interactions are already universal [31]. This suggests that hard computational problems that can be formulated as a universal Hamiltonian can be solved by a simulator that is designed for finding the global minimum of such Hamiltonian. In particular, the XY model is a quadratic constrained optimization model, which is an NP-hard problem for non-convex and sufficiently dense matrices [32, 29].

A more traditional use of analogue Hamiltonian simulators has been based on modelling electrons as they move on a lattice generated by the periodic array of atomic cores. To elucidate such a behaviour ultra cold atomic condensates were loaded into optical lattices such as cubic-type lattices [33], superlattice structures [34, 35], triangular

[36], hexagonal [36, 37] and Kagome [38] lattices. Polariton graphs can easily produce such or any other ordered or disordered lattice. It was recently shown that a linear periodic chain of exciton-polariton condensates demonstrate not only various classical regimes: ferromagnetic, antiferromagnetic and frustrated spiral phases, but also at higher pumping intensities bring about novel exotic phases that can be associated with spin liquids [39]. Relationship between the energy spectrum of the XY Hamiltonian and the total number of condensed polariton particles has been established in Ref.[40] where it was shown that “particle mass residues” of successive polariton states (defined as the difference between the masses of the individual condensates and the total mass) that occur with increasing excitation density above condensation threshold are an accurate approximation of the XY Hamiltonian’s energy spectrum. Therefore, polariton graph condensate system may represent not only the ground state but also the spectral gap of the XY model.

Our paper is organised as follows. In Section 2 we consider the mean-field model of polariton condensates and derive analytical solutions for a single condensate. We establish the phase mapping of a polariton graph into the XY model in Section 3. In Section 4 we derive the Kuramoto model that describes the dynamics of the phases of the polariton condensates and show its relevance to the XY model. We conclude with the discussions in Section 5.

2. An approximate analytical solution for a single condensate

The mean field of polariton condensates can be modelled [41, 42] in association with atomic lasers by writing a driven-dissipative Gross-Pitaevskii equation (aka the complex Ginzburg-Landau equation (cGLE)) for the condensates wavefunction $\psi(\mathbf{r}, t)$:

$$i\hbar \frac{\partial \psi}{\partial t} = -\frac{\hbar^2}{2m} (1 - i\eta_d \mathcal{R}) \nabla^2 \psi + U_0 |\psi|^2 \psi + \hbar g_R \mathcal{R} \psi + \frac{i\hbar}{2} (R_R \mathcal{R} - \gamma_C) \psi \quad (1)$$

coupled to the rate equation for the density of the hot exciton reservoir, $\mathcal{R}(\mathbf{r}, t)$:

$$\frac{\partial \mathcal{R}}{\partial t} = (\gamma_R + R_R |\psi|^2) \mathcal{R} + P(\mathbf{r}). \quad (2)$$

In these equations m is polariton effective mass, U_0 and g_R are the strengths of effective polariton-polariton and polariton-exciton interactions, respectively, η_d is the energy relaxation coefficient specifying the rate at which gain decreases with increasing energy, R_R is the rate at which the reservoir excitons enter the condensate, γ_C is the rates of the condensate losses, γ_R is the redistribution rate of reservoir excitons between the different energy levels, and P is the pumping into the reservoir. In the limit $\gamma_R \gg \gamma_C$ one can replace Eq. 2 with the stationary state for the reservoir $\mathcal{R} = P(\mathbf{r})/(\gamma_R + R_R |\psi|^2)$.

To non-dimensionalize the cGLE we use $\psi \rightarrow \sqrt{\hbar^2/2mU_0\ell_0^2} \Psi$, $\mathbf{r} \rightarrow \ell_0 \mathbf{r}$, $t \rightarrow 2mt\ell_0^2/\hbar$, where we choose $\ell_0 = 1\mu$ m and introduce the notations $g = 2g_R/R_R$, $\gamma = m\gamma_C\ell_0^2/\hbar$, $p = m\ell_0^2 R_R P(\mathbf{r})/\hbar\gamma_R$, $\eta = \eta_d \hbar/mR_R\ell_0^2$, and $b = R_R \hbar^2/2m\ell_0^2 \gamma_R U_0$.

The dimensionless form of Eqs. (1)-(2) becomes the cGLE with a saturable nonlinearity

$$i \frac{\partial \Psi}{\partial t} = -(1 - i\eta n_R) \nabla^2 \Psi + |\Psi|^2 \Psi + g n_R \Psi + i(n_R - \gamma) \Psi, \quad (3)$$

$$n_R = p(\mathbf{r}) / (1 + b|\Psi|^2). \quad (4)$$

By taking the Taylor expansion for small $|\Psi|^2$ in the expression for the reservoir n_R we arrive at the more standard cGLE

$$i \frac{\partial \Psi}{\partial t} = -(1 - i\eta p) \nabla^2 \Psi + (1 - pb) |\Psi|^2 \Psi + gp \Psi + i(p - \gamma - pb|\Psi|^2) \Psi, \quad (5)$$

where, in the view of smallness of η we dropped $g\eta|\Psi|^2$ term. We can compare the relative strength of nonlinearities in Eqs. (3-4) and (5) depending of the physical quantities that define b . By taking the values the system parameters typically accepted for GaAs microcavities [43, 44, 26] $\hbar R_R = 0.1 \text{meV} \cdot \mu\text{m}^2$, $U_0 = 0.02 - 0.04 \text{meV} \cdot \mu\text{m}^2$ we obtain $b = 2 - 4/\gamma R p s$. With γ_R on the order of 1ps^{-1} we have b of the order of the real nonlinearity.

We consider the asymptotics and approximations of the steady state solutions for a single radially symmetric Gaussian pumping profile $p(r) = p_0 \exp(-\sigma r^2)$, where p_0 is the maximum pumping intensity and σ characterises the inverse width of the Gaussian. The Madelung transformation $\Psi = \sqrt{\rho} \exp[iS]$ relates the wavefunction to density $\rho = |\Psi|^2$ and velocity $\mathbf{u} = \nabla S$. Separating the real and imaginary parts of Eqs. (3-4) we arrive at the mass continuity and the Bernoulli equations:

$$\frac{1}{r\rho} \frac{d(r\rho u)}{dr} = \frac{p(r)}{1 + b\rho} \left(1 + \frac{\eta(r(\sqrt{\rho})')'}{r\sqrt{\rho}} - \eta u^2 \right) - \gamma, \quad (6)$$

$$\mu = -\frac{(\sqrt{\rho})''}{\sqrt{\rho}} - \frac{(\sqrt{\rho})'}{r\sqrt{\rho}} + u^2 + \rho + \frac{p(r)}{1 + b\rho} \left(g - \frac{\eta}{r\rho} \frac{d(r\rho u)}{dr} \right). \quad (7)$$

Away from the pumping spot, where $p(r) = 0$, the velocity $u = |\mathbf{u}|$ is given by the outflow wavenumber $k_c = \text{const}$ with $r\rho_r + \rho = -\gamma\rho r/k_c$, which can be integrated to yield $\rho \sim \exp[-r\gamma/k_c]/r$. From Eq. (7) at infinity we obtain $\mu = k_c^2 - \gamma^2/4k_c^2$. In the view of their asymptotic behaviour the condensate density and velocity can be approximated by

$$\rho(r) = \frac{a_0}{\gamma r \exp(\gamma r k_c^{-1}) k_c^{-1} + \xi - \gamma r/k_c + a_3 r^3}, \quad (8)$$

and

$$u(r) = k_c \tanh(lr/k_c), \quad (9)$$

utilizing their behaviour at the origin and infinity and introducing parameters ξ , a_0 , a_3 , and l that define the parametric family of solutions. Their values should be found from the governing equations via matching asymptotics, as shown below.

We neglect η in the view of its smallness and substitute the expressions for the density, velocity and the pumping profile into Eqs. (6-7). By expanding the resulting expressions about $r = 0$ and setting the term to the order $\mathcal{O}(r^2)$ to zero we obtain the equations that define the unknown parameters ξ , a_0 , a_3 , l and k_c in terms of the system

parameters $g, b, \gamma, p_0, \sigma$. The leading order expansion of Eq. (6) and the first order expansion of Eq. (7) fix ξ and a_3 as

$$\xi = \frac{a_0 b (2l + \gamma)}{p_0 - 2l - \gamma}, \quad a_3 = -\frac{\gamma^3}{2k_c^2}. \quad (10)$$

The expansion to $\mathcal{O}(r^2)$ of Eq. (6) determines k_c as

$$k_c^2 = [4a_0 b l^3 p_0 (2l + \gamma) + 3\gamma^2 (8l^3 - 12l^2 (p_0 - \gamma) + (p_0 - \gamma)^2 \gamma + 2l(2p_0^2 - 5p_0 \gamma + 3\gamma^2))] / (3a_0 b p_0 \sigma (2l + \gamma)^2) \quad (11)$$

Finally, the expansions to $\mathcal{O}(r^2)$ of Eq. (7) define the remaining parameters a_0 and l through two nonlinear equations

$$k_c^2 = \frac{a_0}{\xi} + \frac{\gamma^2 (\xi + 8)}{4k_c^2 \xi} + \frac{g p_0 \xi}{a_0 b + \xi}, \quad (12)$$

$$l^2 = \frac{a_0 \gamma^2}{k_c^2 \xi^2} + \frac{5\gamma^4}{k_c^4 \xi^2} - \frac{4\gamma^4}{3k_c^4 \xi} - \frac{a_0 b g p_0 \gamma^2}{k_c^2 (a_0 b + \xi)^2} + \frac{g p_0 \sigma \xi}{a_0 b + \xi}. \quad (13)$$

Equations (8) and (9) with the parameters defined by Eqs. (10-13) for the given system parameters g, b, γ and the pumping parameters p_0 and σ fully specify the approximate analytical solution of Eqs. (6-7). Figure 2 shows the comparison of the approximate analytical solutions (solid lines) given by Eqs. (8-9) and the numerical solutions (dashed lines) of Eqs. (6-7) for $b = 1.5, \gamma = 0.2, g = 0.5$ and two sets of parameters specifying the pumping profile (a) $p_0 = 5, \sigma = 0.2$ and (b) $p_0 = 10, \sigma = 0.4$. The values specifying velocity are $k_c = 1.65885, l = 0.541858$ for (a) and $k_c = 1.99239, l = 0.909976$ for (b). Both analytical density and velocity profiles are in an excellent agreement with the numerical solutions.

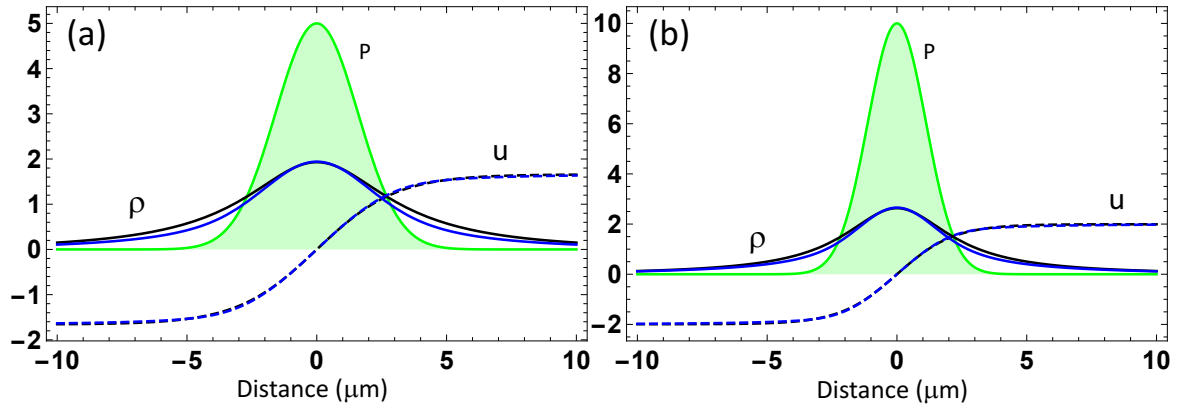


Figure 2. Approximate analytical (blue lines) and numerical (black lines) solutions for density (solid lines) and velocity (dashed lines) of Eq. (5) for the pumping profile given by $p(r) = p_0 \exp(-\sigma r^2)$ (green shaded area). The system parameters are $b = 1.5, \gamma = 0.2, g = 0.5$ and (a) $\sigma = 0.2, p_0 = 5$; (b) $\sigma = 0.4, p_0 = 10$.

3. Mapping of phases into the classical XY Model

In the previous section we obtained solutions of the governing equation Eq. (5) for a single pumping Gaussian spot. Spatial light modulator can be used to pump condensates at the vertices of a distributed graph via

$$p(\mathbf{r}) = \sum_{i=1}^N p_i \exp[-\sigma_i |\mathbf{r} - \mathbf{r}_i|^2], \quad (14)$$

where p_i stands for the pumping intensity at the center of the spot at position $\mathbf{r} = \mathbf{r}_i$. In what follows we shall assume that all vertices are pumped identically, so that $p_i = p_0$, $\sigma_i = \sigma$ for all $i = 1, \dots, N$. To the leading order and assuming that all condensates are well-separated we can approximate the resulting condensate wave function, ψ_N , as $\Psi_N(\mathbf{r}, t) \approx \sum_{i=1}^N \Psi_0(|\mathbf{r} - \mathbf{r}_i|) \exp(i\theta_i)$, where $\Psi_0 = \Psi_0(r)$ is the solution of the stationary Eq. (5) for a single localized radially symmetric condensate pumped by $p(r) = p_0 \exp(-\sigma r^2)$, found in the previous section

$$\Psi_0(r) = \sqrt{\rho_0(r)} \exp \left[i \frac{k_c^2}{l} \log \cosh \left(\frac{l}{k_c} r \right) \right], \quad (15)$$

where $\rho_0(r)$ is given by Eq. (8). To find the total amount of matter \mathcal{M} we write

$$\mathcal{M} = \int |\Psi_N|^2 d\mathbf{r} = \frac{1}{(2\pi)^2} \int |\tilde{\Psi}_N(\mathbf{k})|^2 d\mathbf{k}, \quad (16)$$

$$\tilde{\Psi}_N(\mathbf{k}) = \int \exp(-i\mathbf{k} \cdot \mathbf{r}) \Psi_N(\mathbf{r}) d\mathbf{r} = \tilde{\Psi}_0(k) \sum_{i=1}^N \exp(i\mathbf{k} \cdot \mathbf{x}_i + i\theta_i), \quad (17)$$

where $\tilde{\Psi}_0(k) = 2\pi \int_0^\infty \Psi_0(r) J_0(kr) r dr$ and J_0 is the Bessel function. The total mass becomes

$$\mathcal{M} = 2\pi N \int_0^\infty |\Psi_0|^2 r dr + \sum_{i<j} J_{ij} \cos(\theta_i - \theta_j), \quad (18)$$

$$J_{ij} = \frac{1}{\pi} \int_0^\infty |\tilde{\Psi}_0(k)|^2 J_0(k|\mathbf{r}_i - \mathbf{r}_j|) k dk. \quad (19)$$

Since the system maximizes the total number of particles given by Eq. (18), this is equivalent to minimising the XY Hamiltonian functional $\mathcal{H}_{XY} = -\sum_{i<j}^n J_{ij} \cos \theta_{ij}$ [29]. The main contribution to the integral defining $\tilde{\Psi}_0(k)$ is from $k = k_c$, where k_c is the outflow wavevector from the pumping site fully determined by the pumping profile [28, 29].

Figure 3 shows the density contour plots (normalised) and the spin orientations (arrows) representing the relative phases, with the incoherent pump spots located at the vertices. The coupling between the adjacent polariton sites can be made ferromagnetic ($J_{ij} > 0$, solid lines) or antiferromagnetic ($J_{ij} < 0$, dashed lines) by either varying the distance between the pumping spots, as illustrated in Figs. 3(a-e,g) or by changing the pumping parameters of the individual spots as shown in Fig. 3(f). Spin configuration, such as ferromagnetic, where all $J_{ij} > 0$ [Fig. 3(a)], rhombic, where all horizontal $J_{ij} > 0$ [Fig. 3(b)], spiral 1, where all $J_{ij} < 0$ [Fig. 3(c)] and spiral 2, where all horizontal $J_{ij} < 0$ [Fig. 3(d)] can be obtained by controlling independently the distance

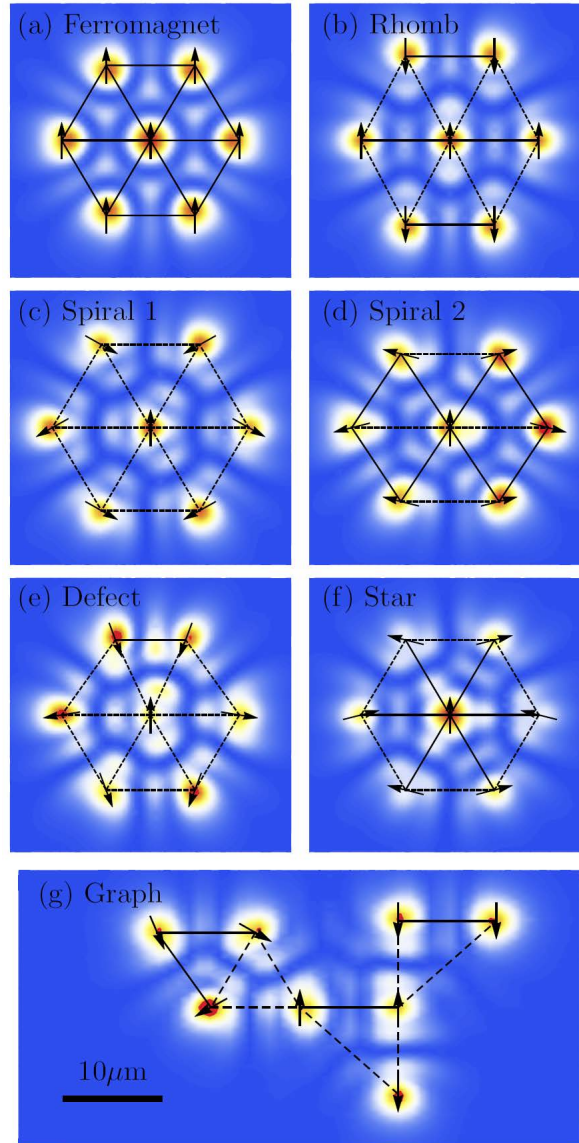


Figure 3. Theoretical prediction of classical magnetic spin configurations showing contour plots of the normalised density and spin orientations (arrows): (a) ferromagnet, with all $J_{ij} > 0$, (b) rhomb, with all horizontal $J_{ij} > 0$, (c) spiral 1, with all $J_{ij} < 0$, (d) spiral 2, with all horizontal $J_{ij} < 0$, (e) defect, with a single ferromagnetic coupling (top edge), (f) star, with $J_{ij} > 0$ from central vertex to all its neighbours, (g) graph, fully disordered system. The density contour plots show $|\Psi|^2$, with $\Psi = \sum \Psi_i$. The individual wave functions Ψ_i are analytic approximations as described in the text with $b = 1.5, g = 0.5, p_0 = 3, \sigma = 0.2$.

and therefore the coupling along two directions of the lattice. In atomic optical lattices, this can be achieved via an elliptical shaking of the lattice and the spin configurations on Fig. 3(a-d) were demonstrated for trapped atomic condensates [30].

The ultimate advantage of polariton graphs for quantum simulations is the potential to control both the sign and the strength of any coupling, J_{ij} , by tuning the distance between polariton sites, or the characteristics of the pumping spots (the intensity, p_0 , or the inverse width of the Gaussian, σ) leading to more exotic phases. We illustrate the control over an individual J_{ij} on the seven-vertex graphs of Figs. 3(e,f). In Figure 3(e) we utilise control over an individual J_{ij} by tuning the distance between two vertices and introduce a single ferromagnetic coupling (defect edge) into an otherwise antiferromagnetic configuration. In Figure 3(f) we control the coupling of a single polariton site (central vertex) to all its neighbours by tuning the intensity of its pumping spot and switch them to ferromagnetic in an otherwise antiferromagnetically coupled graph (star configuration). Finally, polariton graphs allow for fully disordered systems to be addressed as shown in Fig. 3(g).

4. Kuramoto Model

The cGLE can be reformulated as the Kuramoto model which is a paradigm for a spontaneous emergence of collective synchronization and that has been widely used to understand the topological organization of real complex systems from neural networks to power grids [45]. In this context the polariton lattice describes collective dynamics of N coupled phase oscillators with phases $\theta_i(t)$, characterized by the natural frequencies ω_i which are associated with the chemical potential of individual condensates.

To show this we adopt a two-mode model that neglects the spacial variations and represents the network of interacting polariton condensates via the radiative couplings \mathcal{J}_{ij} between i th and j th condensates

$$i\Psi_{it} = |\Psi_i|^2\Psi_i + \left(\frac{(g+i)p}{1+b|\Psi_i|^2} - i\gamma\right)\Psi_i + i\sum_j \mathcal{J}_{ij}\Psi_j. \quad (20)$$

We neglect the blueshift g and without loss of generality let $\gamma = 1$. For the densities and phases of the individual condensates we obtain

$$\begin{aligned} \frac{1}{2}\dot{\rho}_i(t) &= \frac{p\rho_i}{1+b\rho_i} - \rho_i + \sum \mathcal{J}_{ij}\sqrt{\rho_i\rho_j}\cos\theta_{ij} \\ \dot{\theta}_i(t) &= -\rho_i - \sum \mathcal{J}_{ij}\frac{\sqrt{\rho_j}}{\sqrt{\rho_i}}\sin\theta_{ij}. \end{aligned} \quad (21)$$

The radiative coupling \mathcal{J}_{ij} is due to the interference of the condensates from different pumping spots [46], and are such that $\mathcal{J}_{ij} \ll \rho_i$ for any j . First, we shall assume that the density number dynamics is faster than the phase dynamics, so that the densities acquire the instantaneous steady state values $\rho_i = \rho = (p-1)/b$ to the leading order in \mathcal{J}_{ij} . In this case we get the equations of the phase dynamics represented by the Kuramoto model:

$$\dot{\theta}_i(t) = -\rho - \sum \mathcal{J}_{ij}\sin\theta_{ij}. \quad (22)$$

The equilibria of system (22) are the stationary points of the potential energy landscape

$$V(\theta) = \rho \sum_{i=1}^N \theta_i - \frac{1}{2} \sum_{i,j=1}^N \mathcal{J}_{ij} \cos \theta_{ij}, \quad (23)$$

so that the Kuramoto model (22) describes the gradient flow to the minima of $V(\theta)$ and, therefore, minimizes the XY Hamiltonian.

Next, we will allow for the density variations and consider two spots only. For the system with just two condensates we introduce the average density $R = (\rho_1 + \rho_2)/2$ and the half density difference $z = (\rho_1 - \rho_2)/2$ for which the system reduces to three equations:

$$\begin{aligned} \dot{\theta}_{12} &= -2z - 2\mathcal{J}_{12} \frac{R}{\sqrt{R^2 - z^2}} \sin \theta_{12}, \\ \dot{R} &= p[(R+z)Q_+ + (R-z)Q_-] - 2R + 2\mathcal{J}_{12}\sqrt{R^2 - z^2} \cos \theta_{12}, \\ \dot{z} &= p[(R+z)Q_+ - (R-z)Q_-] - 2z, \end{aligned} \quad (24)$$

where we defined $Q_{\pm} = (1 + b(R \pm z))^{-1}$. Assuming that z and \mathcal{J}_{12} are small compared to R we can expand these equations in small parameters z and \mathcal{J}_{12} and consider the steady state for R , which to the leading order is $R = (p-1)/b$. Eliminating z from Eq. (24) we see that θ_{12} satisfies the second-order differential equation

$$\ddot{\theta}_{12} + 2\left(1 - \frac{1}{p} + \mathcal{J}_{12} \cos \theta_{12}\right)\dot{\theta}_{12} = -4\left(1 - \frac{1}{p}\right)\mathcal{J}_{12} \sin \theta_{12}. \quad (25)$$

As the pumping increases from the threshold value of p_{th} the oscillations between two condensates become damped with the rate proportional to $2\left(1 - p^{-1} + \mathcal{J}_{ij} \cos \theta_{12}\right)$. The relative phases lock to 0 or π difference depending on whether $\mathcal{J}_{12} > 0$ or $\mathcal{J}_{12} < 0$, respectively. This again agrees with the minimization of the XY Model, which for two pumping spots is $H_{XY} = -\mathcal{J}_{12} \cos \theta_{12}$ with minimum at $\theta_{12} = 0$ if $\mathcal{J}_{12} > 0$ and π if $\mathcal{J}_{12} < 0$.

Despite many numerical and analytical studies of the Kuramoto model on complex networks of different architectures there are many questions remain, in particular, on the dependence of synchronization on the system size, the relaxation dynamics of the model, the effects of time-delayed couplings and stochastic noise. In a large heterogeneous network may exist various synchronization phase transitions. These effects as well as the effect of other correlations between intrinsic dynamical characteristics and local topological properties could be addressed by the polariton graph simulator.

5. Conclusions

In conclusion, we discussed polariton graphs as an analog platform for minimizing the XY Hamiltonian and therefore emulating classical spin model with a potential of solving computationally hard problems. We demonstrated that the search for the global ground state of a polariton graph is equivalent to the minimisation of the XY Hamiltonian $H_{XY} = -\sum J_{ij} \cos(\theta_{ij})$. The theoretically predicted phase transitions explained the

recent experiments for small and large scale polariton graphs [28, 26, 29]. Polariton graphs offer the scalability of optical lattices, together with the potential to study disordered systems and to control both the sign and the strength of the coupling for each edge independently. Phase transitions in polariton graphs occur at the global ground state. With the recent advances in the field of polariton condensates, such as room temperature operation [47] and condensation under electrical pumping [48], polariton graph based simulators offer unprecedented opportunities in addressing NP-complete and hard problems, topological quantum information processing and the study of exotic quantum phase transitions. Finally, we would like to emphasize that the word "quantum" could be attached to our proposal for a simulator to reflect the statistical nature of polariton condensates. The process of Bose-Einstein condensation is inherent to quantum statistics where a large fraction of bosons occupies the lowest quantum state, at which point macroscopic quantum phenomena become apparent. The use of the classical mean-field equations to describe the kinetics of the condensate does not negate the quantum statistic nature of its existence. At the same time, the proposed simulator has a quantum speed-up which is associated with the stimulated process of condensation i.e. an accelerated relaxation to the global ground quantum state.

6. References

- [1] Feynman R R 1982 Simulating physics with computers *Int. J. Theor. Phys.* **21** 467
- [2] Greiner M, Mandel O, Esslinger T, Hansch T and Bloch I. 2002 Quantum phase transition from a superfluid to a Mott insulator in a gas of ultracold atoms *Nature* **415** 39
- [3] Lewenstein M, Sanpera A, Ahufinger V, Damski B, Sen A and Sen U 2007 Ultracold atomic gases in optical lattices: mimicking condensed matter physics and beyond *Advances in Physics* **56** 243
- [4] Saffman M, Walker T G, and Molmer K 2010 Quantum information with Rydberg atoms *Rev. Mod. Phys.* **82** 2313
- [5] Simon J, Bakr W S, Ma R, Tai M E, Preiss Ph M and Greiner M 2011 Quantum simulation of antiferromagnetic spin chains in an optical lattice *Nature* **472** 307
- [6] Esslinger T 2010 Fermi-Hubbard Physics with Atoms in an Optical Lattice *Annu. Rev. Condens. Matter Phys.* **1** 129
- [7] Northup T E and Blatt R 2014 Quantum information transfer using photons *Nature Photonics* **8** 356
- [8] Kim K, Chang M-S, Korenblit S, Islam R, Edwards E E, Freericks J K, Lin G-D, Duan L-M, and Monroe C 2010 Quantum simulation of frustrated Ising spins with trapped ions *Nature* **465** 590
- [9] Lanyon B P, Hempel C, Nigg D, Müller M, Gerritsma R, Zuhriinger F, Schindler P, Barreiro J T, Rambach M, Kirchmair G, Hennrich M, Zoller P, Blatt R, Roos C F 2011 Universal digital quantum simulation with trapped ions *Science* **334** 57
- [10] Córcoles A D, Magesan E, Srinivasan S J, Cross A W, Steffen M, Gambetta J M and Chow J M 2015 Demonstration of a quantum error detection code using a square lattice of four superconducting qubits, *Nature Commun.* **6** 6979
- [11] Utsunomiya S, Takata K and Yamamoto Y 2011 Mapping of Ising models onto injection-locked laser systems, *Opt. Express* **19** 18091
- [12] Marandi A, Wang Z, Takata K, Byer R L, and Yamamoto Y, Network of time-multiplexed optical parametric oscillators as a coherent Ising machine *Nature Photonics* **8** 937
- [13] Nixon M, Ronen E, Friesem A A, and Davidson N 2013 Observing geometric frustration with thousands of coupled lasers *Phys. Rev. Lett.* **110** 184102

- [14] Bloch I, Dalibard J and Nascimbéne S 2012 Quantum simulations with ultracold quantum gases *Nature Physics* **8** 267
- [15] Weisbuch C, Nishioka M, Ishikawa A and Arakawa, Y 1992 Observation of the coupled exciton-photon mode splitting in a semiconductor quantum microcavity. *Phys. Rev. Lett.* **69** 3314
- [16] Kasprzak J *et al.* 2006 Bose-Einstein condensation of exciton polaritons *Nature* **443** 409
- [17] Deng H, Weihs G, Santori C, Bloch J and Yamamoto Y 2002 Condensation of Semiconductor Microcavity Exciton Polaritons *Science* **298** 199
- [18] Keeling J and Berloff N G 2011 Exciton-polariton condensation *Contemporary Physics* **52** 131
- [19] Carusotto I and Ciuti C 2013 Quantum Fluids of Light *Rev. Mod. Phys.* **85** 299
- [20] Nardin G, Léger Y, Pietka B, Morier-Genoud F, Deveaud-Plédran B 2010 Phase-resolved imaging of confined exciton-polariton wave functions in elliptical traps *Phys. Rev. B* **82** 045304
- [21] Galbiati M *et al* 2012 Polariton Condensation in Photonic Molecules *Phys. Rev. Lett.* **108** 126403
- [22] Lai C W *et al* 2007 Coherent zero-state and p-state in an exciton-polariton condensate array *Nature* **450** 529
- [23] Balili R, Hartwell V, Snoke D, Pfeiffer L and West K 2007 Bose-Einstein Condensation of Microcavity Polaritons in a Trap *Science* **316** 1007
- [24] Miller D A B, Chemla D S, Damen T C, Gossard A C, Wiegmann W, Wood T H, Burrus C A 1984 Band-Edge Electroabsorption in QuantumWell Structures: The Quantum-Confined Stark Effect *Phys. Rev. Lett.* **53** 2173
- [25] Keeling J and Berloff N G 2011 Controllable half-vortex lattices in an incoherently pumped polariton condensate arXiv:1102.5302
- [26] Tosi G, Christmann G, Berloff N G, Tsotsis P, Gao T, Hatzopoulos Z, Savvidis P G and Baumberg J J 2012 Sculpting oscillators with light within a nonlinear quantum fluid *Nature Physics* **8** 190
- [27] Tosi G, Christmann G, Berloff N G, Tsotsis P, Gao T, Hatzopoulos Z, Savvidis P G and Baumberg J J 2013 Geometrically locked vortex lattices in semiconductor quantum fluids *Nature Comm* **3** 1243
- [28] Ohadi H, Gregory R L, Freearge T, Rubo Y G, Kavokin A V, Berloff N G and Lagoudakis P G 2016 Nontrivial Phase Coupling in Polariton Multiplets, *Phys. Rev. X* **6** 031032
- [29] Berloff N G, Silva M, Kalinin K, Askitopoulos A, Topfer J D, Cilibrizzi P, Langbein W and Lagoudakis P G 2017 Realizing the classical XY Hamiltonian in polariton simulators to appear *Nature Materials*, also arXiv:1607.06065
- [30] Struck J *et al* 2011 Quantum simulation of frustrated classical magnetism in triangular optical lattices, *Science* **333** 996
- [31] Cuevas G D and Cubitt T S 2016 Simple universal models capture all classical spin physics. *Science* **351** 1180
- [32] Pardalos P M and Vavasis S A 1991 Quadratic programming with one negative eigenvalue is NP-hard *J.Global Optim.* **1** 15
- [33] Greiner M, Bloch I, Mandel M O, Hansch T W and Esslinger T 2001 Exploring phase coherence in a 2D lattice of Bose-Einstein condensates *Phys. Rev. Lett.* **87** 160405
- [34] Sebby-Strabley J, Anderlini M, Jessen P and Porto J 2006 Lattice of double wells for manipulating pairs of cold atoms *Phys. Rev. A* **73** 033605
- [35] Folling S *et al* 2007 Direct observation of second-order atom tunnelling *Nature* **448** 1029
- [36] Becker C *et al* 2010 Ultracold quantum gases in triangular optical lattices *New J. Phys.* **12** 065025
- [37] Tarruell L, Greif D, Uehlinger T, Jotzu G and Esslinger T 2012 Creating, moving and merging Dirac points with a Fermi gas in a tunable honeycomb lattice *Nature* **483** 302
- [38] Jo G-B *et al* 2011 Ultracold atoms in a tunable optical kagome lattice *Phys. Rev. Lett.* **108** 045305
- [39] Kalinin K, Lagoudakis P G and Berloff N G 2017 Exotic states of matter with polariton chains, in review by *Phys. Rev. Letts.* (2017)
- [40] Exotic states of matter with polariton chains, in review by *Phys. Rev. Letts.* (2017)
- [41] Wouters M and Carusotto I 2007 Excitations in a nonequilibrium Bose-Einstein condensate of exciton polaritons, *Phys. Rev. Lett.* **99** 140402

- [42] Keeling J and Berloff N G 2008 Spontaneous rotating vortex lattices in a pumped decaying condensate *Phys. Rev. Lett.* **100** 250401
- [43] Manni F, Lagoudakis K G, Liew T C H, André R and Deveaud-Plédran B 2011 Spontaneous pattern formation in a polariton condensate *Phys. Rev. Lett.* **107** 106401
- [44] Lagoudakis K G *et al* 2008 Quantized vortices in an exciton-polariton condensate *Nat. Phys.* **4** 706
- [45] Rodrigues F A, Peron T K, Ji P and Kurths J 2016 The Kuramoto model in complex networks *Physics Reports*, **610** 1
- [46] Aleiner I L, Altshuler B L and Rubo Y G 2012 Radiative coupling and weak lasing of exciton-polariton condensates *Phys. Rev. B* **85** 121301(R)
resulting from finite inertia in coupled oscillator systems *Phys. Rev. Letts.* **78** 2104
oscillators with hysteretic responses *Physica D: Nonlinear Phenomena* **100** 279 **13** R135 (2001)
- [47] Plumhof J D, Stöferle T, Mai L, Scherf U and Mahrt R F 2014 Room-temperature Bose-Einstein condensation of cavity exciton-polaritons in a polymer *Nat. Mat.* **13** 247
- [48] Schneider C *et al* 2013 An electrically pumped polariton laser *Nature* **497** 348